PHYSICAL REVIEW B **91**, 161306(R) (2015)

Spin-polarized quantum well states on $Bi_{2-x}Fe_xSe_3$

Michael M. Yee,[1,*] Z.-H. Zhu,[1,*] Anjan Soumyanarayanan,[1] Yang He,[1] Can-Li Song,[1] Ekaterina Pomjakushina,[2] Zaher Salman,[3] Amit Kanigel,[4] Kouji Segawa,[5] Yoichi Ando,[5] and Jennifer E. Hoffman[1,†]

[1]*Department of Physics, Harvard University, Cambridge, Massachusetts 02138, USA*

[2]*Laboratory for Development and Methods, Paul Scherrer Institute, CH-5232 Villigen PSI, Switzerland*

[3]*Laboratory for Muon Spin Spectroscopy, Paul Scherrer Institute, CH-5232 Villigen PSI, Switzerland*

[4]*Department of Physics, Technion-Israel Institute of Technology, Haifa 32000, Israel*

[5]*Institute of Scientific and Industrial Research, Osaka University, Ibaraki, Osaka 567-0047, Japan*

(Received 22 January 2015; revised manuscript received 1 April 2015; published 24 April 2015)

Low temperature scanning tunneling microscopy is used to image the doped topological insulator $Bi_{2-x}Fe_xSe_3$. Interstitial Fe defects allow the detection of quasiparticle interference, and the reconstruction of the empty state band structure. Quantitative comparison between measured data and density functional theory calculations reveals the unexpected coexistence of quantum well states (QWSs) with topological surface states (TSSs) on the atomically clean surface of $Bi_{2-x}Fe_xSe_3$. Spectroscopic measurements quantify the breakdown of linear dispersion due to hexagonal warping. Nonetheless, both QWSs and TSSs remain spin polarized and protected from backscattering to almost 1 eV above the Dirac point, suggesting their utility for spin-based applications.

DOI: 10.1103/PhysRevB.91.161306 PACS number(s): 71.20.−b, 68.37.Ef, 71.15.Mb, 73.20.At

Topological insulators (TIs), recently discovered materials with insulating bulk and topologically protected helical Dirac surface states, have generated widespread excitement due to proposed applications such as dissipationless spintronics, ambipolar transistors, and fault-tolerant quantum computers [1–3]. Many of these applications hinge on the predicted ability to preserve spin information without backscattering. Bi_2Se_3 has attracted particular attention due to the accessibility of its Dirac point within a relatively large ∼300 meV bulk band gap [4], and the availability of additional quantum well surface states [5–13] which may be spin polarized by a large Rashba effect [14,15]. However, spin-polarized quantum well states (QWSs) depend sensitively on adsorbents, and have not been observed on clean surfaces. More generally, little is known about the empty state band structure of Bi_2Se_3, which is inaccessible to angle-resolved photoemission spectroscopy (ARPES). For applications involving both topological surface states (TSSs) and QWSs, it remains crucial to characterize the high-energy extent to which they remain linearly dispersing, spin polarized, and protected against surface-bulk scattering [16,17] and backscattering [18].

Scanning tunneling microscopy and spectroscopy (STM/STS) can provide real space images of both filled and empty states and their local relationship to surface and near-surface impurities. STM also provides access to momentum space information via quasiparticle interference (QPI) imaging. When quasiparticle states of energy ε scatter elastically from impurities, the interference between initial and final quasiparticle wave vectors $\boldsymbol{k_i}$ and $\boldsymbol{k_f}$ can result in a standing wave pattern with wave vector $\boldsymbol{q} = \boldsymbol{k_f} - \boldsymbol{k_i}$ at energy ε. The observed dispersion of $\boldsymbol{q}(\varepsilon)$, and the inversion of $\boldsymbol{q}(\varepsilon)$ to find $\boldsymbol{k}(\varepsilon)$, has established QPI as a reliable k-space probe [19]. Indeed, QPI imaging has been used to demonstrate the protection against backscattering [20,21] and the high-energy breakdown of linear dispersion in pristine Bi_2Te_3 [22], as well as the onset of backscattering in $Bi_{2-x}Fe_xTe_3$ [23]. However, dispersing QPI in Bi_2Se_3 has been elusive [17,24,25], appearing only in a limited energy range with inconsistent velocity [26–28]. Therefore, the high-energy band structure and scattering mechanisms of Bi_2Se_3 are unknown.

Here we address these issues using STM measurements of bulk $Bi_{2-x}Fe_xSe_3$, coupled with density functional theory (DFT). Previous experiments focused on the magnetic properties of bulk Fe dopants via transport [30], ARPES [31], or muon spin rotation (μSR) and magnetization measurements [32]; or adsorbed Fe [6,33–35]; or Fe dopants in thin films [36]. In this STM study of bulk $Bi_{2-x}Fe_xSe_3$, we report multiple dispersing QPI modes, which give access to the full high-energy band structure, up to 1 eV above the Dirac point. Furthermore, we provide real space evidence for the coexistence of QWSs and TSSs on the pristine surface of a bulk material. Finally, we demonstrate the absence of backscattering of the QWSs, and we report the relationship of scattering between TSSs, QWSs, and bulk. All of these observations are enabled by surface potential confinement due to the presence of interstitial Fe defects in the van der Waals (vdW) gap between adjacent Bi_2Se_3 quintuple layers (QLs).

We studied $Bi_{2-x}Fe_xSe_3$ single crystals with nominal $x = 0$ [37] and 0.07 [32]. Samples were cleaved in vacuum at $T \sim 40$ K and immediately inserted into our home-built STM at 4 K. Topographic images were obtained in constant current mode (I_s) at a fixed sample bias (V_s). Differential conductance dI/dV, proportional to the local density of states, was measured at a fixed tip-sample distance using a standard lock-in technique. Theoretical calculations were performed using the linearized augmented-plane-wave method in the WIEN2K packages [38] and an *ab initio* DFT slab method [39].

Topographic images of flat terraces of $Bi_{2-x}Fe_xSe_3$ reveal multiple species of threefold symmetric defects, segregated into three distinct micron-scale regions, and typified in Figs. 1(a)–1(c). Region I is dominated by the same Se vacancies and Bi_{Se} antisite defects seen in "pristine" Bi_2Se_3 [40,41]. Region II is dominated by Fe substitutions in the top two

*The first two authors contributed equally to this work.

†jhoffman@physics.harvard.edu

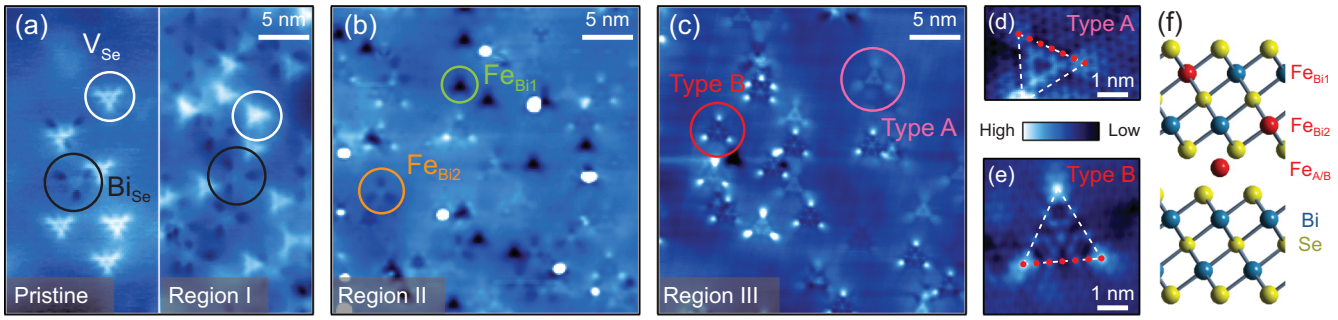

FIG. 1. (Color online) (a)–(c) STM topographies of pristine Bi_2Se_3 [(a) left] and three regions of $Fe_{0.07}Bi_{1.93}Se_3$ [(a) right, (b), and (c)]. Six types of impurities, circled in (a)–(c), are segregated into three distinct micron-scale regions in Fe-doped samples. Region I is characterized by the same impurities seen in pristine samples, i.e., Se vacancies (V_{Se}) and Bi_{Se} antisites. Region II contains Fe substitutions at two different Bi sites (Fe_{Bi1} and Fe_{Bi2}). Region III contains two types of Fe interstitials in the van der Waals gap (type A and type B). (d), (e) High resolution topographies of type-A and type-B Fe interstitials. Their spatial signature has a similar vertex-to-vertex distance of $6a_0$, indicated by red dots, where $a_0 = 4.14$ Å is the Se-Se lattice constant [29]. (f) Crystal structure of Bi_2Se_3 with Fe dopants shown in red. Experimental conditions: (a) left, $V_s = 0.4$ V, $I_s = 30$ pA; (a) right, $V_s = 0.5$ V, $I_s = 50$ pA; (b) $V_s = 1$ V, $I_s = 20$ pA; (c) $V_s = 0.55$ V, $I_s = 100$ pA; (d), (e) $V_s = 0.5$ V, $I_s = 100$ pA.

Bi layers, Fe_{Bi1} and Fe_{Bi2} [36]. Region III is dominated by two larger defects, detailed in Figs. 1(d)–1(e). The first ("type A"), centered between topmost Se atoms, was identified as an interstitial Fe [36]. The second ("type B"), centered on a topmost Se atom, has not been previously observed. Based on their vertex-to-vertex distance of $6a_0 = 2.5$ nm, and the assumption that their perturbations propagate primarily along the $pp\sigma$ chains extending out and upwards to the surface [40], we conclude that both defects in region III are Fe interstitials at inequivalent sites within the vdW gap beneath the top QL. The density of atomic Fe defects in regions II and III is lower than the nominal doping by a factor of ∼100, but occasional Fe clusters do appear [42].

The low Fe concentration is consistent with the small size of Fe^{3+} compared to Bi^{3+}, which makes it difficult to dope [43]. The spatial separation of distinct impurities can be understood from calculations showing that Fe substitution in Bi_2Se_3 is allowed only in Se-rich conditions [43,44], which also inhibit the formation of Se vacancies [45,46]. On the other hand, Fe interstitials are not energetically favored under any Bi/Se ratio. Such interstitials may appear due to kinetic constraint where the local growth temperature is too low for Fe to overcome the energy barrier to substitute for Bi [43].

We now focus on the electronic structure in region III. The dI/dV maps in Figs. 2(a)–2(c) display clear QPI patterns, particularly around the type-B interstitials. The QPI has three

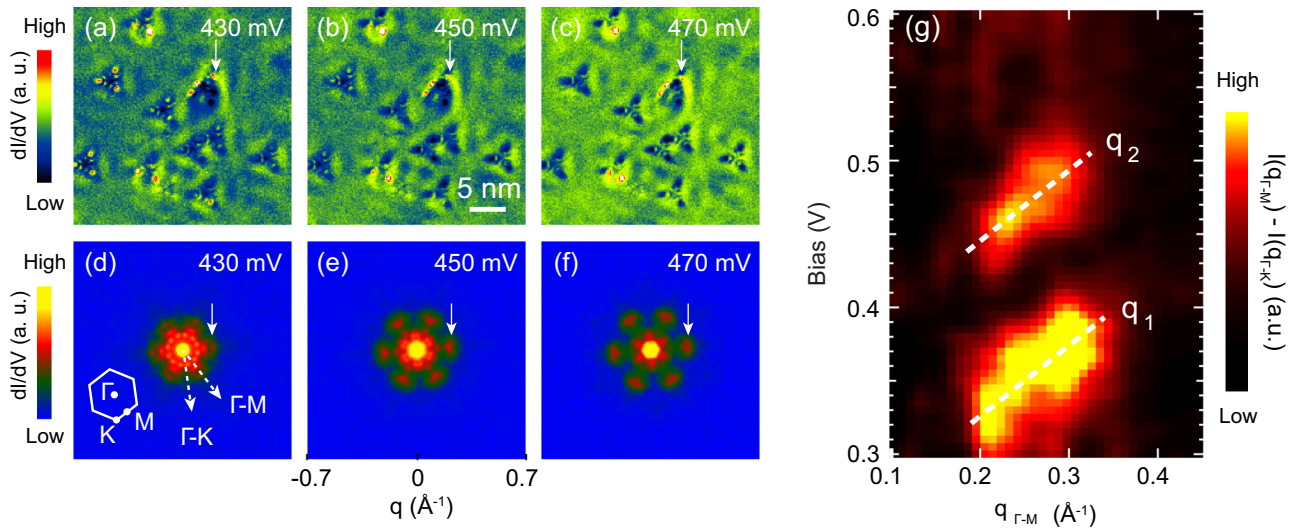

FIG. 2. (Color online) (a)–(c) dI/dV maps over a 30×30 nm^2 region at the indicated bias. (d)–(f) Fourier transform (FT) dI/dV maps at varying bias over a 60×60 nm^2 region encompassing the area of (a)–(c). A white arrow points to the dispersive Γ-M scattering mode. The inset in (d) is a schematic of the surface Brillouin zone with the high symmetry points. Data were acquired at $T = 6$ K, $V_s = 0.6$ V, $I_s = 300$ pA, $V_{rms} = 7$ mV (a)–(c), $V_{rms} = 5$ mV (d)–(f). (g) Fourier linecut showing q_1 and q_2 scattering modes. The Fourier intensity of the linecut in the Γ-K direction is subtracted from the Fourier intensity of the linecut in the Γ-M direction for the FT dI/dV maps shown in (d)–(f). The white dashed lines highlight the linear dispersions of q_1 and q_2 whose detectable range is limited approximately by the scattering center separation (∼3–5 nm, corresponding to $q_{min} \sim 0.2$ Å^{-1}) and the scattering center size (∼$6a_0$, corresponding to $q_{max} \sim 0.3$ Å^{-1}).

remarkable features. First, the scattering modes appear at unexpectedly high-energy levels, almost 1 eV above the Dirac point. At such high energies the band structure of Bi_2Se_3 was expected to consist of bulk continuum states and was not expected to have a well-defined TSS [20,47]. Second, the Fourier transform dI/dV maps in Figs. 2(d)–2(f) show no dispersing Γ-K modes, but two Γ-M modes (q_1 and q_2) which disperse with similar slope but ∼0.1 eV relative offset. To better isolate the dispersing Γ-M modes from the long-wavelength dopant disorder (presumed to be isotropic), we plot $I(q_{\Gamma\text{-}M}) - I(q_{\Gamma\text{-}K})$ as a function of bias voltage V_s and wave vector q in Fig. 2(g). Third, the high-energy Γ-M mode velocities, $v_{q_M} \sim 1.1$–1.3 eV Å, are substantially smaller than the ARPES-measured TSS velocity at low energies near the Dirac point ($v_{DP} = 3.5$ eV Å) [48], reflecting a sharp kink in the band dispersion along Γ-M at intermediate energy, as shown in Figs. 3(a) and 3(b). Finally, we emphasize that QPI is observed only in region III where Fe interstitials are present.

We argue that the parallel Γ-M scattering modes in Fig. 2(g) demonstrate a remarkable extension of both TSSs and QWSs, far above the energy range accessible to ARPES [5–15]. To support this claim, Fig. 3(a) shows our calculated band structure in a 5QL slab, the minimal system which prevents interactions between top and bottom surfaces, but also supports QWSs with depths comparable to fits of ARPES data [5,7,14] and the independently measured bulk screening length [49]. (We also checked that the calculated band velocity here is a robust feature, nearly independent of the slab thickness [42].) Constant energy contours (CECs) in Figs. 3(c)–3(e) show the hexagonal warping [50] which emerges at high energy in both TSSs and QWSs, along with the expected spin texture of these states [15]. Similar to previous studies on Bi_2Te_3 [20–22], scattering in Bi_2Se_3 is expected to depend on the warping of the CECs, with a dominant mode emerging between two adjacent M-oriented corners of the hexagram (denoted by q_M). Because these corners are separated by an angle of $\pi/3$, the velocity of q_M should well approximate the band velocity along the Γ-M direction, $v_{q_M} = v_{k(\Gamma\text{-}M)}$ [42]. Furthermore, the warping of TSSs and QWSs in Figs. 3(c)–3(e) evolves similarly, but shifted in energy, akin to the parallel scattering modes observed in Fig. 2(g). Indeed, Fig. 3(b) shows excellent quantitative agreement between our STM scattering data and DFT calculations, confirming that q_1 and q_2 modes arise from scattering between adjacent M-oriented corners of the CECs of the TSS and QWS1, respectively.

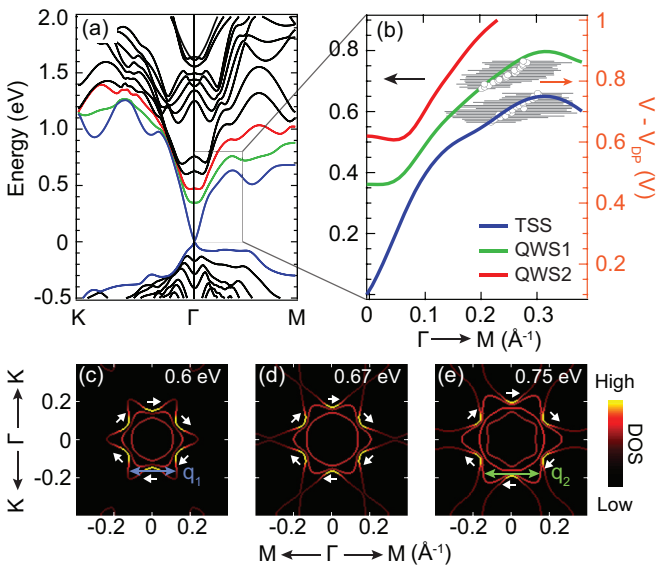

FIG. 3. (Color online) (a) Calculated band structure of a 5QL slab with the TSSs and first two QWSs in blue, green, and red, respectively. (b) Comparison between the calculated high-energy Γ-M bands and the measured dispersions of the two QPI modes. The gray circles and horizontal bars represent the centers and widths of Gaussian fits to the intensity profile at each bias in Fig. 2(g). The measured Dirac point bias V_{DP} is -0.35 V [42]. The energy offset between left and right axes represents a rigid band shift which arises from our approximation of the near-surface potential gradient as a square well in our DFT calculations. (c)–(e) Constant energy contours at energies spanning the transition from dominant TSS scattering (q_1) to dominant QWS1 scattering (q_2). The color scale is defined by the density of states of the top five atomic layers in a 5QL slab. The expected spin texture due to Rashba-like spin splitting (not included in the calculation) is sketched by white arrows.

Spectroscopic evidence further supports the presence of QWS. In Fig. 4(a), the spatially averaged dI/dV spectrum from region III shows three distinct kinks over the same energy range as the observed QPI. These kinks are qualitatively well reproduced in Fig. 4(b), which shows the momentum-integrated density of states from the DFT band structure in Fig. 3(a). By comparison with Fig. 3(a), we see that the three kinks in the DOS occur near the three energies where the linear dispersions of the TSS, QWS1, and QWS2 bands break down.

Despite the breakdown of linear dispersion and the onset of bulk bands, both TSSs and QWSs remain unexpectedly robust against backscattering. We observe no dispersing Γ-K modes throughout the measured energy range, which rules out backscattering and indicates the spin polarization of the TSS and Rashba spin splitting of the QWS [51] to ∼1 eV above the Dirac point. We observe one weak, nondispersing

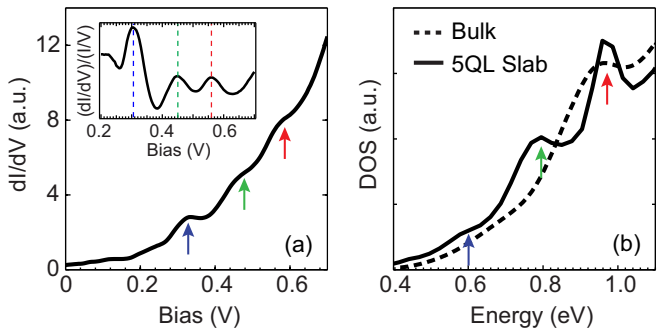

FIG. 4. (Color online) (a) Spatially averaged dI/dV spectrum ($V_s = 0.7$ V, $I_s = 0.34$ nA, and $V_{rms} = 5.6$ mV) showing three prominent kinks at 0.30, 0.45, and 0.56 V. The position variation of each kink is less than 20 mV over a 100×100 nm^2 nm region. The inset shows the normalized dI/dV spectrum: $(dI/dV)/(I/V)$. (b) Calculated density of states (DOS) from the bulk (dashed line) and a 5QL slab (solid line) of Bi_2Se_3 (with $V_{DP} = 0$ in the calculation). The slab DOS profile has kinks similar to those observed in the experimental spectrum in (a).

Γ-K mode, $q_K \sim 0.44$ Å^{-1}, around $V_s = 300$–400 meV [42]. Previous studies ascribed nondispersing QPI modes to surface-bulk scattering in Bi_2Se_3 [17]. However, our observed q_K corresponds closely to the $2\sqrt{3}a_0$ distance from the bright center to the lobes of the type-B interstitial Fe defects, which is determined simply by the bond geometry of the impurity [40]. We therefore find no evidence of backscattering or surface-bulk scattering deteriorating the TSSs or the QWSs at high energy in Bi_2Se_3.

Finally, we comment on the origin of QWSs. Previously observed QWSs in Bi_2Se_3 were believed to arise from band bending due to charged adsorbents [7–9,14,15], or vdW gap expansion due to burrowing adsorbents [10,52]. Here we have reported evidence of QWSs at the clean surface of a bulk crystal. Fe interstitials may induce surface potential confinement and further give rise to QWSs at the clean surface of bulk $Bi_{2-x}Fe_xSe_3$ by two independent mechanisms: (1) their ionization to Fe^{3+} would donate three electrons to induce downward band bending [36]; (2) their cores would physically expand the vdW gap. Either mechanism supposes vertical dopant inhomogeneity, in keeping with the lateral inhomogeneity demonstrated in Fig. 1. (The tip itself cannot be responsible for the the observed QWSs, because the tip's positive bias cannot cause the downward band bending required to induce QWSs in the bulk conduction band.)

In conclusion, our STM/STS study of $Bi_{2-x}Fe_xSe_3$ provides fundamental information about the empty state band structure of Bi_2Se_3. Scattering from interstitial Fe defects allowed QPI imaging and band structure reconstruction up to 1 eV above the Dirac point, from which we draw three main conclusions. First, quantitative comparison between our QPI data and DFT calculations proves the unexpected appearance of QWSs, coexisting with TSSs, at the clean surface of a bulk material. These well-defined surface states persist to almost 1 eV above the Dirac point, overlapping by ~0.6 eV with the bulk conduction band, but showing no evidence of backscattering. Second, distinctive kinks in dI/dV spectra reveal the breakdown of linear dispersion for TSSs and the first two QWSs. The high-energy velocity is $3\times$ smaller than the velocity near the Dirac point, and is consistent with our DFT calculations. Third, the absence of dispersing Γ-K scattering demonstrates the protection of both TSSs and QWSs against backscattering, well beyond the breakdown of linear dispersion, even in the presence of sparse Fe dopants. Our results suggest that interstitial defects in the vdW gap of Bi_2Se_3 can lead to the coexistence of protected spin-polarized QWSs and TSSs over a wide energy range, far outside the bulk band gap. These discoveries bode well for the controlled use of spins in future devices.

We benefited from computational resources provided by Ilya Elfimov. This research was supported by the U.S. National Sciences Foundation under Grant No. DMR-110623. M.M.Y. was supported by an NSERC PGS-D fellowship, Z.-H.Z. was supported by an NSERC PDF fellowship, A.S. was supported by A*STAR, Y.H. was supported by the New York Community Trust–George Merck fund, and C.L.S. was supported by the Lawrence Golub fellowship at Harvard University. Work at Osaka University was supported by JSPS (KAKENHI 25220708) and AFOSR (AOARD 124038).

[1] M. Z. Hasan and C. Kane, Colloquium: Topological insulators, Rev. Mod. Phys. **82**, 3045 (2010).

[2] X.-L. Qi and S.-C. Zhang, Topological insulators and superconductors, Rev. Mod. Phys. **83**, 1057 (2011).

[3] Y. Ando, Topological insulator materials, J. Phys. Soc. Jpn. **82**, 102001 (2013).

[4] D. Hsieh, Y. Xia, D. Qian, L. Wray, J. H. Dil, F. Meier, J. Osterwalder, L. Patthey, J. G. Checkelsky, N. P. Ong, A. V. Fedorov, H. Lin, A. Bansil, D. Grauer, Y. S. Hor, R. J. Cava, and M. Z. Hasan, A tunable topological insulator in the spin helical Dirac transport regime, Nature (London) **460**, 1101 (2009).

[5] M. Bianchi, D. Guan, S. Bao, J. Mi, B. B. Iversen, P. D. C. King, and P. Hofmann, Coexistence of the topological state and a two-dimensional electron gas on the surface of Bi_2Se_3, Nat. Commun. **1**, 128 (2010).

[6] L. A. Wray, S.-Y. Xu, Y. Xia, D. Hsieh, A. V. Fedorov, Y. S. Hor, R. J. Cava, A. Bansil, H. Lin, and M. Z. Hasan, A topological insulator surface under strong coulomb, magnetic and disorder perturbations, Nat. Phys. **7**, 32 (2010).

[7] H. M. Benia, C. Lin, K. Kern, and C. R. Ast, Reactive chemical doping of the Bi_2Se_3 topological insulator, Phys. Rev. Lett. **107**, 177602 (2011).

[8] Z.-H. Zhu, G. Levy, B. Ludbrook, C. N. Veenstra, J. A. Rosen, R. Comin, D. Wong, P. Dosanjh, A. Ubaldini, P. Syers, N. P. Butch, J. Paglione, I. S. Elfimov, and A. Damascelli, Rashba spin-splitting control at the surface of the topological insulator Bi_2Se_3, Phys. Rev. Lett. **107**, 186405 (2011).

[9] M. Bianchi, R. C. Hatch, J. Mi, B. B. Iversen, and P. Hofmann, Simultaneous quantization of bulk conduction and valence states through adsorption of nonmagnetic impurities on Bi_2Se_3, Phys. Rev. Lett. **107**, 086802 (2011).

[10] M. Ye, S. V. Eremeev, K. Kuroda, M. Nakatake, S. Kim, Y. Yamada, E. E. Krasovskii, E. V. Chulkov, M. Arita, H. Miyahara, T. Maegawa, K. Okamoto, K. Miyamoto, T. Okuda, K. Shimada, H. Namatame, M. Taniguchi, Y. Ueda, and A. Kimura, Relocation of the topological surface state of Bi_2Se_3 beneath the surface by Ag intercalation, arXiv:1112.5869.

[11] C. Chen, S. He, H. Weng, W. Zhang, L. Zhao, H. Liu, X. Jia, D. Mou, S. Liu, J. He, Y. Peng, Y. Feng, Z. Xie, G. Liu, X. Dong, J. Zhang, X. Wang, Q. Peng, Z. Wang, S. Zhang, F. Yang, C. Chen, Z. Xu, X. Dai, Z. Fang, and X. J. Zhou, Robustness of topological order and formation of quantum well states in topological insulators exposed to ambient environment, Pro. Natl. Acad. Sci. U.S.A. **109**, 3694 (2012).

[12] T. Valla, Z.-H. Pan, D. Gardner, Y. S. Lee, and S. Chu, Photoemission spectroscopy of magnetic and nonmagnetic impurities on the surface of the Bi_2Se_3 topological insulator, Phys. Rev. Lett. **108**, 117601 (2012).

[13] S. Roy, H. L. Meyerheim, A. Ernst, K. Mohseni, C. Tusche, M. G. Vergniory, T. V. Menshchikova, M. M. Otrokov, A. G. Ryabishchenkova, Z. S. Aliev, M. B. Babanly, K. A. Kokh, O. E. Tereshchenko, E. V. Chulkov, J. Schneider, and J. Kirschner, Tuning the Dirac point position in Bi_2Se_3(0001) via surface carbon doping, Phys. Rev. Lett. **113**, 116802 (2014).

[14] P. D. C. King, R. C. Hatch, M. Bianchi, R. Ovsyannikov, C. Lupulescu, G. Landolt, B. Slomski, J. H. Dil, D. Guan, J. L. Mi, E. D. L. Rienks, J. Fink, A. Lindblad, S. Svensson, S. Bao, G. Balakrishnan, B. B. Iversen, J. Osterwalder, W. Eberhardt, F. Baumberger, and P. Hofmann, Large tunable Rashba spin splitting of a two-dimensional electron gas in Bi_2Se_3, Phys. Rev. Lett. **107**, 096802 (2011).

[15] M. S. Bahramy, P. D. C. King, A. de la Torre, J. Chang, M. Shi, L. Patthey, G. Balakrishnan, P. Hofmann, R. Arita, N. Nagaosa, and F. Baumberger, Emergent quantum confinement at topological insulator surfaces, Nat. Commun. **3**, 1159 (2012).

[16] S. R. Park, W. S. Jung, C. Kim, D. J. Song, C. Kim, S. Kimura, K. D. Lee, and N. Hur, Quasiparticle scattering and the protected nature of the topological states in a parent topological insulator Bi_2Se_3, Phys. Rev. B **81**, 041405 (2010).

[17] S. Kim, M. Ye, K. Kuroda, Y. Yamada, E. E. Krasovskii, E. V. Chulkov, K. Miyamoto, M. Nakatake, T. Okuda, Y. Ueda, K. Shimada, H. Namatame, M. Taniguchi, and A. Kimura, Surface scattering via bulk continuum states in the 3D topological insulator Bi_2Se_3, Phys. Rev. Lett. **107**, 056803 (2011).

[18] W.-C. Lee, C. Wu, D. P. Arovas, and S.-C. Zhang, Quasiparticle interference on the surface of the topological insulator Bi_2Te_3, Phys. Rev. B **80**, 245439 (2009).

[19] M. F. Crommie, C. P. Lutz, and D. M. Eigler, Imaging standing waves in a two-dimensional electron gas, Nature (London) **363**, 524 (1993).

[20] T. Zhang, P. Cheng, X. Chen, J.-F. Jia, X. Ma, K. He, L. Wang, H. Zhang, X. Dai, Z. Fang, X. Xie, and Q.-K. Xue, Experimental demonstration of topological surface states protected by time-reversal symmetry, Phys. Rev. Lett. **103**, 266803 (2009).

[21] Z. Alpichshev, J. G. Analytis, J.-H. Chu, I. R. Fisher, Y. L. Chen, Z. X. Shen, A. Fang, and A. Kapitulnik, STM imaging of electronic waves on the surface of Bi_2Te_3: Topologically protected surface states and hexagonal warping effects, Phys. Rev. Lett. **104**, 016401 (2010).

[22] P. Sessi, M. M. Otrokov, T. Bathon, M. G. Vergniory, S. S. Tsirkin, K. A. Kokh, O. E. Tereshchenko, E. V. Chulkov, and M. Bode, Visualizing spin-dependent bulk scattering and breakdown of the linear dispersion relation in Bi_2Te_3, Phys. Rev. B **88**, 161407 (2013).

[23] Y. Okada, C. Dhital, W. Zhou, E. D. Huemiller, H. Lin, S. Basak, A. Bansil, Y.-B. Huang, H. Ding, Z. Wang, S. D. Wilson, and V. Madhavan, Direct observation of broken time-reversal symmetry on the surface of a magnetically doped topological insulator, Phys. Rev. Lett. **106**, 206805 (2011).

[24] T. Hanaguri, K. Igarashi, M. Kawamura, H. Takagi, and T. Sasagawa, Momentum-resolved landau-level spectroscopy of Dirac surface state in Bi_2Se_3, Phys. Rev. B **82**, 081305 (2010).

[25] Z. Alpichshev, R. R. Biswas, A. V. Balatsky, J. G. Analytis, J.-H. Chu, I. R. Fisher, and A. Kapitulnik, STM imaging of impurity resonances on Bi_2Se_3, Phys. Rev. Lett. **108**, 206402 (2012).

[26] J. Wang, W. Li, P. Cheng, C. Song, T. Zhang, P. Deng, X. Chen, X. Ma, K. He, J.-F. Jia, Q.-K. Xue, and B.-F. Zhu, Power-law decay of standing waves on the surface of topological insulators, Phys. Rev. B **84**, 235447 (2011).

[27] H. Beidenkopf, P. Roushan, J. Seo, L. Gorman, I. Drozdov, Y. S. Hor, R. J. Cava, and A. Yazdani, Spatial fluctuations of helical Dirac fermions on the surface of topological insulators, Nat. Phys. **7**, 939 (2011).

[28] T. Zhang, N. Levy, J. Ha, Y. Kuk, and J. A. Stroscio, Scanning tunneling microscopy of gate tunable topological insulator Bi_2Se_3 thin films, Phys. Rev. B **87**, 115410 (2013).

[29] J. Wiese and L. Muldawer, Lattice constants of Bi_2Te_3-Bi_2Se_3 solid solution alloys, J. Phys. Chem. Solids **15**, 13 (1960).

[30] J. J. Cha, J. R. Williams, D. Kong, S. Meister, H. Peng, A. J. Bestwick, P. Gallagher, D. Goldhaber-Gordon, and Y. Cui, Magnetic doping and Kondo effect in Bi_2Se_3 nanoribbons, Nano Lett. **10**, 1076 (2010).

[31] Y. L. Chen, J.-H. Chu, J. G. Analytis, Z. K. Liu, K. Igarashi, H.-H. Kuo, X. L. Qi, S. K. Mo, R. G. Moore, D. H. Lu, M. Hashimoto, T. Sasagawa, S. C. Zhang, I. R. Fisher, Z. Hussain, and Z. X. Shen, Massive Dirac fermion on the surface of a magnetically doped topological insulator, Science **329**, 659 (2010).

[32] Z. Salman, E. Pomjakushina, V. Pomjakushin, A. Kanigel, K. Chashka, K. Conder, E. Morenzoni, T. Prokscha, K. Sedlak, and A. Suter, The nature of magnetic ordering in magnetically doped topological insulator $Bi_{2-x}Fe_xSe_3$, arXiv:1203.4850.

[33] M. R. Scholz, J. Sánchez-Barriga, D. Marchenko, A. Varykhalov, A. Volykhov, L. V. Yashina, and O. Rader, Tolerance of topological surface states towards magnetic moments: Fe on Bi_2Se_3, Phys. Rev. Lett. **108**, 256810 (2012).

[34] T. Schlenk, M. Bianchi, M. Koleini, A. Eich, O. Pietzsch, T. O. Wehling, T. Frauenheim, A. Balatsky, J.-L. Mi, B. B. Iversen, J. Wiebe, A. A. Khajetoorians, P. Hofmann, and R. Wiesendanger, Controllable magnetic doping of the surface state of a topological insulator, Phys. Rev. Lett. **110**, 126804 (2013).

[35] J. Honolka, A. A. Khajetoorians, V. Sessi, T. O. Wehling, S. Stepanow, J.-L. Mi, B. B. Iversen, T. Schlenk, J. Wiebe, N. B. Brookes, A. I. Lichtenstein, P. Hofmann, K. Kern, and R. Wiesendanger, In-plane magnetic anisotropy of Fe atoms on Bi_2Se_3(111), Phys. Rev. Lett. **108**, 256811 (2012).

[36] C.-L. Song, Y.-P. Jiang, Y.-L. Wang, Z. Li, L. Wang, K. He, X. Chen, X.-C. Ma, and Q.-K. Xue, Gating the charge state of single Fe dopants in the topological insulator Bi_2Se_3 with a scanning tunneling microscope, Phys. Rev. B **86**, 045441 (2012).

[37] K. Eto, Z. Ren, A. A. Taskin, K. Segawa, and Y. Ando, Angular-dependent oscillations of the magnetoresistance in Bi_2Se_3 due to the three-dimensional bulk Fermi surface, Phys. Rev. B **81**, 195309 (2010).

[38] P. Blaha, K. Schwarz, G. Madsen, D. Kvasnicka, and J. Luitz, in *An Augmented Plane Wave Plus Local Orbitals Program for Calculating Crystal Properties*, edited by K. Schwarz (Technical University of Wien, Vienna, 2001).

[39] Z.-H. Zhu, C. N. Veenstra, G. Levy, A. Ubaldini, P. Syers, N. P. Butch, J. Paglione, M. W. Haverkort, I. S. Elfimov, and A. Damascelli, Layer-by-layer entangled spin-orbital texture of the topological surface state in Bi_2Se_3, Phys. Rev. Lett. **110**, 216401 (2013).

[40] S. Urazhdin, D. Bilc, S. H. Tessmer, S. D. Mahanti, T. Kyratsi, and M. G. Kanatzidis, Scanning tunneling microscopy of defect states in the semiconductor Bi_2Se_3, Phys. Rev. B **66**, 161306 (2002).

[41] Y. S. Hor, A. Richardella, P. Roushan, Y. Xia, J. G. Checkelsky, A. Yazdani, M. Z. Hasan, N. P. Ong, and R. J. Cava, *p*-type Bi_2Se_3 for topological insulator and low-temperature thermoelectric applications, Phys. Rev. B **79**, 195208 (2009).

[42] See Supplemental Material at http://link.aps.org/supplemental/10.1103/PhysRevB.91.161306 for more experimental data and DFT calculations with various slab thicknesses.

[43] J.-M. Zhang, W. Zhu, Y. Zhang, D. Xiao, and Y. Yao, Tailoring magnetic doping in the topological insulator Bi_2Se_3, Phys. Rev. Lett. **109**, 266405 (2012).

[44] L. B. Abdalla, L. Seixas, T. M. Schmidt, R. H. Miwa, and A. Fazzio, Topological insulator Bi_2Se_3(111) surface doped with transition metals: An *ab initio* investigation, Phys. Rev. B **88**, 045312 (2013).

[45] D. West, Y. Y. Sun, H. Wang, J. Bang, and S. B. Zhang, Native defects in second-generation topological insulators: Effect of spin-orbit interaction on Bi_2Se_3, Phys. Rev. B **86**, 121201 (2012).

[46] L.-L. Wang, M. Huang, S. Thimmaiah, A. Alam, S. L. Bud'ko, A. Kaminski, T. A. Lograsso, P. C. Canfield, and D. D. Johnson, Native defects in tetradymite $Bi_2(Te_xSe_{3-x})$ topological insulators, Phys. Rev. B **87**, 125303 (2013).

[47] S. V. Eremeev, Y. M. Koroteev, and E. V. Chulkov, Effect of the atomic composition of the surface on the electron surface states in topological insulators $A_2^V B_3^{VI}$, JETP Lett. **91**, 387 (2010).

[48] K. Kuroda, M. Arita, K. Miyamoto, M. Ye, J. Jiang, A. Kimura, E. E. Krasovskii, E. V. Chulkov, H. Iwasawa, T. Okuda, K. Shimada, Y. Ueda, H. Namatame, and M. Taniguchi, Hexagonally deformed Fermi surface of the 3D topological insulator Bi_2Se_3, Phys. Rev. Lett. **105**, 076802 (2010).

[49] P. Löptien, L. Zhou, J. Wiebe, A. A. Khajetoorians, J. L. Mi, B. B. Iversen, P. Hofmann, and R. Wiesendanger, Screening and atomic-scale engineering of the potential at a topological insulator surface, Phys. Rev. B **89**, 085401 (2014).

[50] L. Fu, Hexagonal warping effects in the surface states of the topological insulator Bi_2Te_3, Phys. Rev. Lett. **103**, 266801 (2009).

[51] H. Hirayama, Y. Aoki, and C. Kato, Quantum interference of Rashba-type spin-split surface state electrons, Phys. Rev. Lett. **107**, 027204 (2011).

[52] S. V. Eremeev, M. G. Vergniory, T. V. Menshchikova, A. A. Shaposhnikov, and E. V. Chulkov, The effect of van der Waals gap expansions on the surface electronic structure of layered topological insulators, New J. Phys. **14**, 113030 (2012).